BIOENGINEERING

Intracellular spectral recompositioning of light enhances algal photosynthetic efficiency

Weiqi Fu,[1]* Amphun Chaiboonchoe,[1] Basel Khraiwesh,[1,2] Mehar Sultana,[2] Ashish Jaiswal,[1] Kenan Jijakli,[1] David R. Nelson,[1,2] Ala'a Al-Hrout,[3] Badriya Baig,[3] Amr Amin,[3,4] Kourosh Salehi-Ashtiani[1,2]*

Copyright © 2017 The Authors, some rights reserved; exclusive licensee American Association for the Advancement of Science. No claim to original U.S. Government Works. Distributed under a Creative Commons Attribution NonCommercial License 4.0 (CC BY-NC).

Diatoms, considered as one of the most diverse and largest groups of algae, can provide the means to reach a sustainable production of petrochemical substitutes and bioactive compounds. However, a prerequisite to achieving this goal is to increase the solar-to-biomass conversion efficiency of photosynthesis, which generally remains less than 5% for most photosynthetic organisms. We have developed and implemented a rapid and effective approach, herein referred to as intracellular spectral recompositioning (ISR) of light, which, through absorption of excess blue light and its intracellular emission in the green spectral band, can improve light utilization. We demonstrate that ISR can be used chemogenically, by using lipophilic fluorophores, or biogenically, through the expression of an enhanced green fluorescent protein (eGFP) in the model diatom *Phaeodactylum tricornutum*. Engineered *P. tricornutum* cells expressing eGFP achieved 28% higher efficiency in photosynthesis than the parental strain, along with an increased effective quantum yield and reduced nonphotochemical quenching (NPQ) induction levels under high-light conditions. Further, pond simulator experiments demonstrated that eGFP transformants could outperform their wild-type parental strain by 50% in biomass production rate under simulated outdoor sunlight conditions. Transcriptome analysis identified up-regulation of major photosynthesis genes in the engineered strain in comparison with the wild type, along with down-regulation of NPQ genes involved in light stress response. Our findings provide a proof of concept for a strategy of developing more efficient photosynthetic cell factories to produce algae-based biofuels and bioactive products.

INTRODUCTION

Global climate change and impending resource scarcity increasingly make the transition to a bio-based economy a matter of urgency (*1*). Phytoplankton, which is composed of photosynthetic cyanobacteria and microalgae, is essential for global carbon recycling and also for sustaining the marine food chain (*2*). Diatoms, which differ from green algae and plants with respect to accessory pigments and light absorption properties, constitute a major group of microalgae and account for 40% of total organic carbon produced annually in marine ecosystems (*3*). Diatoms are also considered as one of the promising resources for the sustainable production of foods and feeds, bioactive pharmaceuticals, and biofuels (*4*–*7*). Recently, more genetic and genome engineering tools have been developed for the production of various commodities from diatoms, including bioactive natural products, food supplements, specialty chemicals, and biofuels (*8*–*13*). Emerging genetic engineering tools make diatoms good candidates as production platforms for biotechnology (*8*, *11*, *13*).

Intensive cultivation is needed to produce algae-derived bioactive compounds and fine chemicals in both outdoor and indoor culture systems (*14*). For large-scale production using diatoms, energy conversion efficiency is a determining factor for economic feasibility and potential of enclosed photobioreactors (PBRs) also plays a vital role of open ponds (*15*, *16*). Economic viability is based mostly on algal biomass production, in which photosynthetic efficiency is essential for enhancing the productivity of cultures (*17*, *18*). Currently, the photosynthetic capabilities of algal systems are still relatively low (*19*), a factor that increases the overall energy costs and reduces the efficiency of cultivation and harvesting processes with a high environmental burden (*16*). For instance, a recent comprehensive analysis indicated that more fossil energy was consumed than bioenergy produced in most scenarios using a theoretical open raceway pond facility for outdoor cultivation of microalgae (*20*). Among many factors that affect algal growth rates, photolimitation from unfavorable light-dark cycles caused by insufficient mixing and photoinhibition due to oversaturation of light on the surface, both of which exist simultaneously in dense cultures of microalgae, act to limit photosynthetic efficiency and reduce overall biomass productivity (*21*). In diatoms, a key mechanism for the abatement of photoinduced stress is nonphotochemical quenching (NPQ), in which energy-dependent quenching (qE) is the most important part of NPQ in diatoms, because there is no state-transition quenching (qT) and photoinhibitory quenching (qI) is little (*22*). NPQ takes place in the light-harvesting complex (LHC) antennae of photosystem II (PSII), where the excess energy of absorbed light is dissipated as heat (*22*). Therefore, much effort is needed to understand and optimize the light-harvesting system and process to make the prospect of developing diatom cell factory a feasible one.

Under natural light conditions, high-energy blue light usually gets wasted and dissipated as heat if excess light energy is provided on the surface of high-density cultures. However, wasting of light energy may be reduced if the light spectrum can be recompositioned by efficiently converting part of the blue portion of the spectrum to green, which can be harvested by accessory pigments. In diatoms, the carotenoid fucoxanthin absorbs light in the blue-green to yellow-green region of visible spectrum in vivo and transfers the energy to the photosynthetic reaction center (*23*). This light recompositioning in PBRs may also mitigate photoinhibition through the improvement of light distribution internally because the converted green light may penetrate deeper into

[1]Laboratory of Algal, Systems, and Synthetic Biology, Division of Science and Math, New York University Abu Dhabi, P.O. Box 129188, Abu Dhabi, UAE. [2]Center for Genomics and Systems Biology, New York University Abu Dhabi, P.O. Box 129188, Abu Dhabi, UAE. [3]Department of Biology, College of Science, UAE University, P.O. Box 15551, Al Ain, UAE. [4]Department of Zoology, Cairo University, Giza, Egypt.
*Corresponding author. Email: wf21@nyu.edu (W.F.); ksa3@nyu.edu (K.S.-A.)

dense diatom cultures due to a lower absorbance of the green spectral region in comparison with blue light (*23*). Here, we present an approach to improve the photosynthetic efficiency in diatom cells through intracellular spectral recompositioning (ISR) of incoming light and demonstrate that quantum yields of photosynthesis, as well as biomass production, increased substantially by integrating fluorescent protein components into the cells and enhancing the light absorption and redistribution in the PBRs.

RESULTS

ISR of light

Unlike chlorophytes, diatoms contain fucoxanthin molecules as accessory pigments in their LHCs (*23*). These pigments are capable of adjusting the photosynthetic apparatus and shifting the absorption spectrum in response to changes in illumination (*24*–*26*). Our strategy relies on the use of an intracellular fluorophore with blue-green absorption and emission properties to enhance this spectral shifting. This approach can reduce light energy waste under high-intensity illumination and optimize the light-harvesting process for microalgae using engineered controllable fluorescent components, such as an enhanced green fluorescent protein (eGFP) for absorbing blue light and re-emitting green light, allowing photons to be redistributed inside the culture (Fig. 1). When exposed to light in the blue-to-ultraviolet spectrum, GFPs emit green fluorescence, peaking at a wavelength of ~510 nm, which can be efficiently captured by the accessory pigment, fucoxanthin (*23*). Therefore, it is feasible to use a considerable amount of otherwise wasted blue light energy by its conversion into green, which can support photosynthesis in diatoms. In this context, our ISR strategy builds on the diatoms' naturally evolved solution to use green light. Our rationally designed strategy enhances this evolved strategy for optimal use of light under high-intensity light growth conditions that diatoms may be subjected to in industrial production settings.

As proof of principle, we tested a chemogenic approach of ISR by exploiting the high neutral lipid contents of *Phaeodactylum tricornutum* and the availability of lipophilic fluorophores with suitable absorption-emission properties. Direct incorporation (*27*) of fluorescent dyes into diatom culture suspensions was performed with the expectation that the dyes would intercalate into the intracellular lipid vesicles of *P. tricornutum* and absorb and emit the incident blue light as green. Two commercially available lipophilic dyes, BODIPY 505/515 and ATTO 465, were chosen to study their effects on shifting the absorption spectrum of diatom cell suspensions. The addition of both dyes enhanced absorption in blue/green light (figs. S1 and S2). Further, our study found that the diatom cells were stained more efficiently at the same concentration using BODIPY 505/515 (*28*) than other fluorescent dyes, such as ATTO 465, which is a moderately lipophilic dye (fig. S3). To chemically demonstrate ISR, we selected BODIPY 505/515 as a candidate for photosynthetic light spectrum modification for high quantum yield and photostability. The addition of 2.0 μM BODIPY 505/515 in diatom culture showed an increase of biomass production and photosynthetic efficiency by approximately 50% (Fig. 2). This simple strategy worked effectively in short-term cultivation, owing to the good compatibility of BODIPY 505/515 with the accumulated lipids and lipid bodies in diatom cells (Fig. 2B). However, the fluorescence of BODIPY 505/515 dye–stained cells decreased substantially over a short period (that is, 24 hours) under both dark and light-emitting diode (LED) illumination conditions (fig. S4). Although it is not clear whether decomposed derivatives of BODIPY 505/515 dye have adverse effects on diatoms, in the long run, the instability of the dye and its cost, particularly for large industrial-scale applications, makes it a nonoptimal solution for use of ISR.

Engineering *P. tricornutum* cells for developing ISR biogenically

We opted to use an engineered green fluorescent protein with enhanced brightness as the ISR fluorescent component, for its high quantum yield and stability, and engineered *P. tricornutum* cells expressing eGFP (*11*, *29*) using different promoters and subcellular localization strategies (figs. S5 and S6). After selection of Zeocin-resistant transformants and fluorescence analysis, two groups of eGFP transformants—chloroplast-localized eGFP (fig. S5C) and nitrate-inducible eGFP transformants (fig. S5D)—were chosen for further study in flat-panel PBRs.

The chloroplast-localized eGFP transformants displayed a higher growth rate than the wild type (WT) under mixed blue and red lights

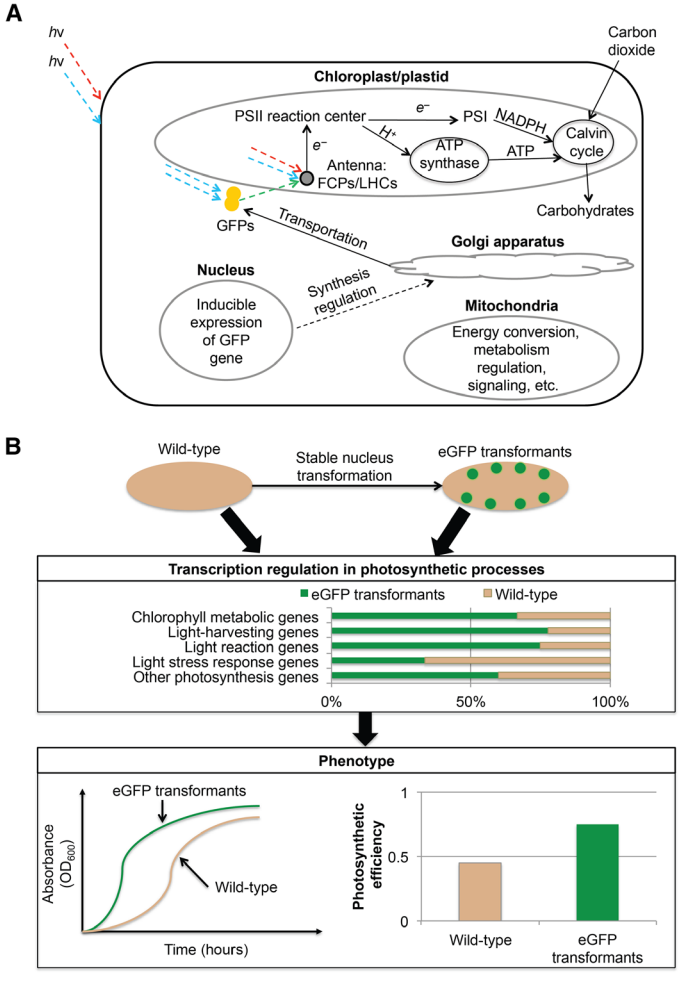

Fig. 1. The ISR strategy for the cultivation of engineered *P. tricornutum* cells. (**A**) Optimization of light spectrum, transfer, and utilization in the eGFP transformant cells. GFPs absorb a portion of wasted blue light and re-emits it as green, which can be captured by LHCs/FCPs and used in PSII. FCPs, fucoxanthin chlorophyll proteins; ATP, adenosine 5′-triphosphate; NADPH, reduced form of nicotinamide adenine dinucleotide phosphate. *hv*, where *h* is the Planck's constant and ν is the frequency of photon, represents the photons. Dashed lines in color represent transmission of light. (**B**) Schematic mechanisms for improving photosynthesis and phenotype characteristics in the eGFP transformants through nucleus transformation. OD_{600}, optical density at 600 nm.

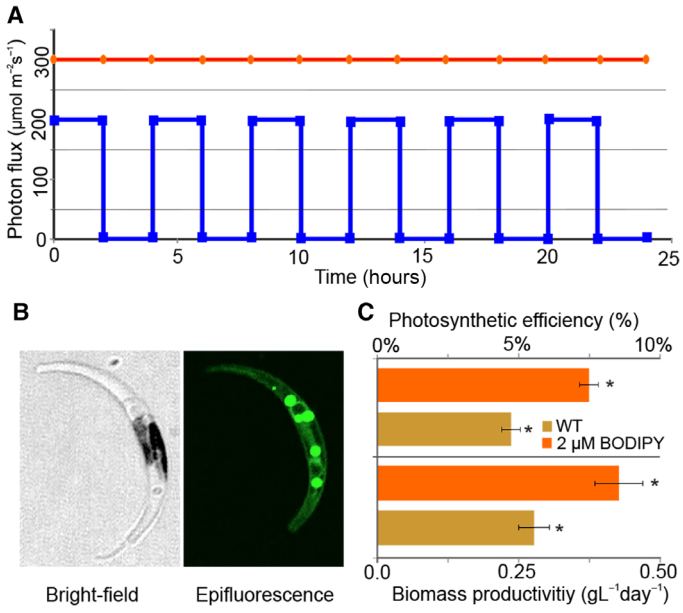

Fig. 2. Cultivation of *P. tricornutum* cells under combined red and blue LED illumination. (**A**) LED illumination applied in the experiments consisted of 25% blue lights and 75% red lights with an overall intensity of 400 μmol photons m^{-2} s^{-1}. (**B**) Fluorescent microscopy images of *P. tricornutum* cells stained with 2.0 μM BODIPY 505/515; stained lipid vesicles are seen as green fluorescence bodies in the image. (**C**) Comparisons of photosynthetic efficiencies in *P. tricornutum* cultures. The values were averaged from three independent experiments. Error bars indicate SEM. *$P < 0.05$, statistically significant difference between the WT and stained cells (with BODIPY).

at 400 μmol photons m^{-2} s^{-1}. No significant difference in growth or photosynthetic efficiency was observed between the chloroplast-localized eGFP transformant and wild-type diatoms at irradiances at or lower than 200 μmol photons m^{-2} s^{-1} (fig. S7). Although emission of green fluorescence from the chloroplast-localized eGFP transformants was only 15-fold higher than the WT *P. tricornutum* (fig. S8A), nitrate-inducible eGFP transformants showed an increase of green fluorescence up to 75-fold higher than the WT in PBRs (fig. S8B); therefore, the nitrate-inducible eGFP transformants are superior to the chloroplast-localized eGFP transformants with respect to eGFP expression (fig. S8), making the former more suitable for this study. Furthermore, the nitrate-inducible eGFP transformant strains exhibited stable and robust green light emission signals during long-term cultivation, and the nitrate-deprived strain could quickly regain high levels of green fluorescence upon resupplementation of nitrate for rapid induction of eGFP expression (fig. S9). These results demonstrate the potential of the strain for large-scale production in industry.

Spectral shifting and emission profiling analysis (Fig. 3, A to C) revealed the expected increase in blue/green light absorption and the distinct emission of green light in the nitrate-inducible eGFP transformants, in which the green fluorescence could be captured by the diatom culture, as evidenced by its absorption spectrum, which displays absorbance in green bandwidth. Growth performance enhancement was assessed with the biogenic ISR strategy (Fig. 3, D and E). Although no significant difference in growth was observed between the eGFP transformants and the WT under a lower light intensity of 50 μmol photons m^{-2} s^{-1}, photosynthetic efficiency in the eGFP transformants was improved by 30% compared to its WT counterpart, and the effective quantum yield in PSII increased by more than 18% under a light intensity of 200 μmol photons m^{-2} s^{-1} (Fig. 3, D and E). Maximal NPQ response measurements showed an NPQ reduction of 0.22 ± 0.05, or approximately 9%, in the eGFP transformants under a light intensity of 200 μmol photons m^{-2} s^{-1} (Fig. 4, A and B). Moreover, under red LED illumination of 200 μmol photons m^{-2} s^{-1}, without any blue light, there was no significant growth difference between the WT and the eGFP transformants (fig. S10).

We performed elemental analysis to determine whether there was a change in composition of dry biomass. The results showed no significant difference in the carbon fraction between WT and eGFP transformant strains (table S1). Because CO_2 is the sole carbon source for diatom growth in our experiments, these data confirm that biomass productivity improvement in the eGFP transformants was due exclusively to the enhancement of carbon fixation and associated photosynthetic productivity. These results indicate that growth enhancement is associated with and is likely due to an increased effective quantum yield (Fig. 3D) and the mitigated photoinhibition, as indicated by reduced NPQ levels in PSII under high-intensity light conditions through light distribution optimization by eGFP.

Evaluation of diatom cultivation in open pond simulators

The described flat-panel PBR experiments demonstrated that the nitrate-inducible eGFP transformants gained a growth advantage over the WT under light stress conditions. Further tests to simulate cultivation of the eGFP transformants in outdoor open ponds were performed in one pond simulators (OPSs) using PBR101 bioreactors (*30*), a recently developed environmental PBR (ePBR), designed to mimic lighting from outdoor raceway pond environments, with a diurnal light cycle (fig. S11). Experiments were conducted to evaluate the production potential with a white LED light spectrum consisting of red, green, and blue lights. The results indicated that, under simulated daily 14:10-hour light/dark cycle growth conditions with a peak intensity of 2000 μmol photons m^{-2} s^{-1}, an intensity that corresponds to the average daily peak intensities in subtropical latitudes, such as the UAE, the eGFP transformants outperformed their WT counterparts in photosynthesis and growth by more than 50%, as evidenced by enhancement of both specific and average growth rates (fig. S12). These results demonstrate that the engineered strains were superior to their WT counterparts in overall biomass production in simulated outdoor cultivation and that the ISR growth enhancement is not limited to high-intensity blue light alone.

Transcriptome sequencing and global analysis of gene expression

To identify transcriptional responses of the cells in the presence and absence of eGFP, we performed RNA sequencing (RNA-seq) to identify differentially expressed genes (DEGs) in both the WT and eGFP transformants cultivated under a light intensity of 200 μmol photons m^{-2} s^{-1} (see Materials and Methods). Specifically, the genome sequence of *P. tricornutum* [ASM15095v2 (2013-07-EBI-Phatr3)] was used as a reference to align the transcriptome reads, and FPKM (fragments per kilobase of transcript per million mapped reads) values were calculated to characterize gene expression in cells (see Materials and Methods). We identified that there were 11,092 genes expressed in both the WT and eGFP transformants, whereas 147 genes were uniquely expressed in eGFP transformants (Fig. 5A and data sets S1 and S2). Among the expressed genes in both strains, a total of 2080 genes were up-regulated and 1906 genes were down-regulated in the eGFP transformants compared to WT with corrected $P < 0.05$ (Fig. 5B and data sets S3 and S4). Although expression with twofold (or above) change in either direction (up or down) was found in more than 1000 genes, a total of 1310 genes displayed less than 1.5-fold change across the two strains at the aforementioned *P* value.

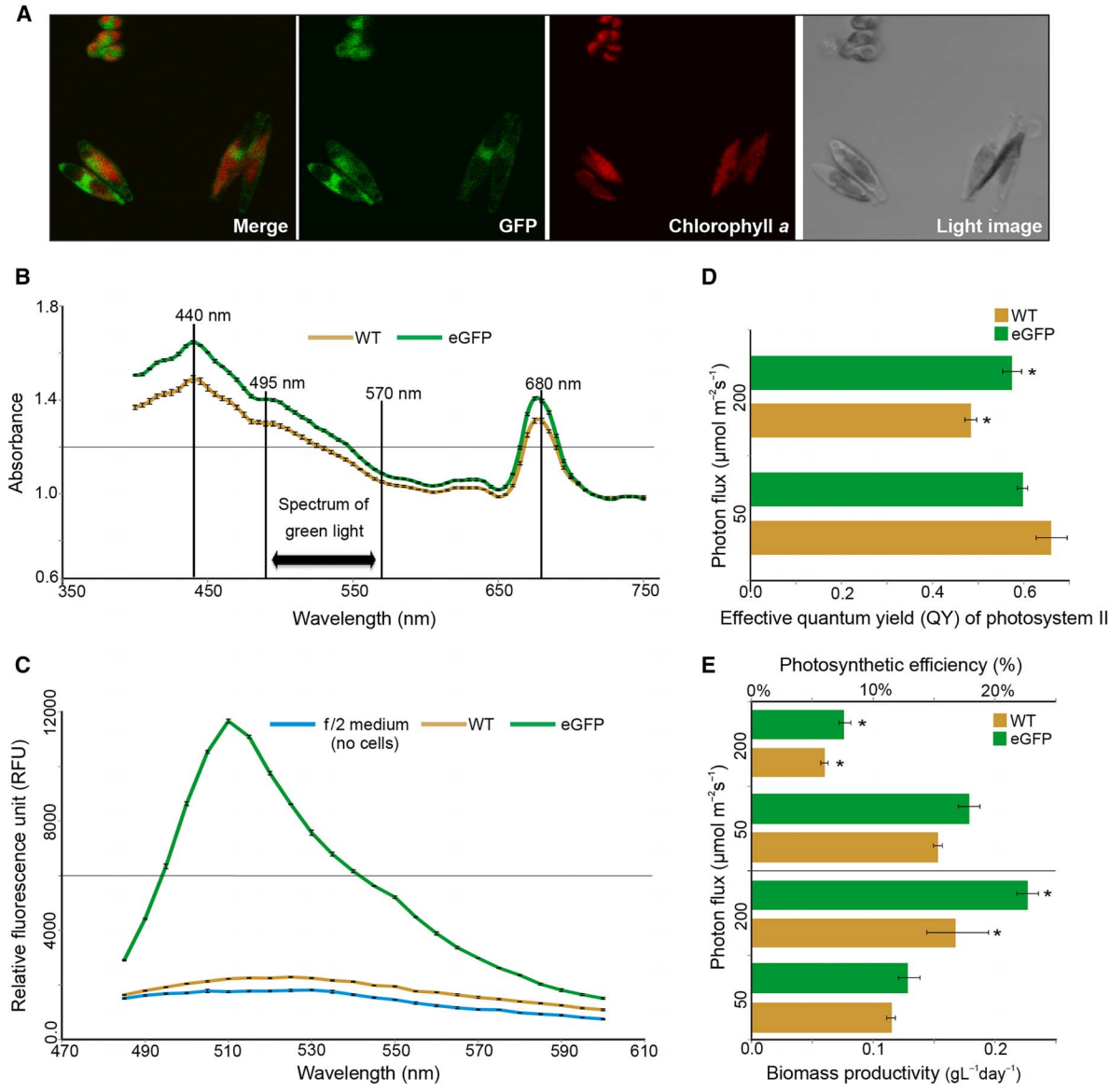

Fig. 3. Engineered diatoms for enhanced growth performance and energy conversion efficiency through the ISR strategy. (**A**) Fluorescent microscopy images of the nitrate-inducible eGFP transformants with construct pPha-NR/eGFP. (**B**) Shifting of absorption spectra in the eGFP transformants. (**C**) Emission spectra of the WT and eGFP transformants ranging from 485 to 600 nm. Excitation wavelength, 455 nm. (**D**) Quantum yields of PSII in WT and transformants using flat-panel PBRs. Values were averaged from three independent experiments. *$P < 0.05$, statistically significant difference between the WT and the transformants. (**E**) Photosynthetic energy conversion efficiencies in the WT and transformants using flat-panel PBRs. Values were averaged from three independent experiments. Error bars indicate SEM. *$P < 0.05$, statistically significant difference between the WT and the transformants.

We performed RNA-seq on the WT cultivated under a low-light intensity condition with a photon flux of 50 μmol photons m^{-2} s^{-1} in comparison with the high-light intensity (200 μmol photons m^{-2} s^{-1}) condition. DEGs were also identified in the WT under high- and low-intensity light conditions. A total of 11,271 genes were detected in the WT samples, and there were 11,019 genes expressed in the WT under both high- and low-light conditions (Fig. 5C). Among the expressed genes in both conditions, a total of 2259 genes were up-regulated under high-intensity light condition relative to low-intensity light condition, and 2004 genes were down-regulated (Fig. 5D and data set S5). In addition to the *LHCX1* gene (data set S6), the other two LHC subfamilies, that is, *LHCR* genes encoding chlorophyll α-binding proteins and *LHCF* genes encoding fucoxanthin chlorophyll *a*/*c*-binding proteins, including *LHCR2*, *LHCR4*, *LHCR12*, *LHCR14*, *LHCF1*, *LHCF5*, *LHCF7*, *LHCF8*, and *LHCF14*, were also highly down-regulated in the WT under light stress condition in comparison with the low-intensity light condition. We note that suppression of these genes in the eGFP transformants was partially or wholly mitigated under the same light stress condition (data set S7). Further, we observed a similar pattern of mitigation of light stress–induced suppression in core PSII genes, for example, *PsbM* (encoding the PSII reaction center protein M), *PsbO*, and *PsbU* (responsible for oxygen-evolving complex functioning and stabilization) (data set S6).

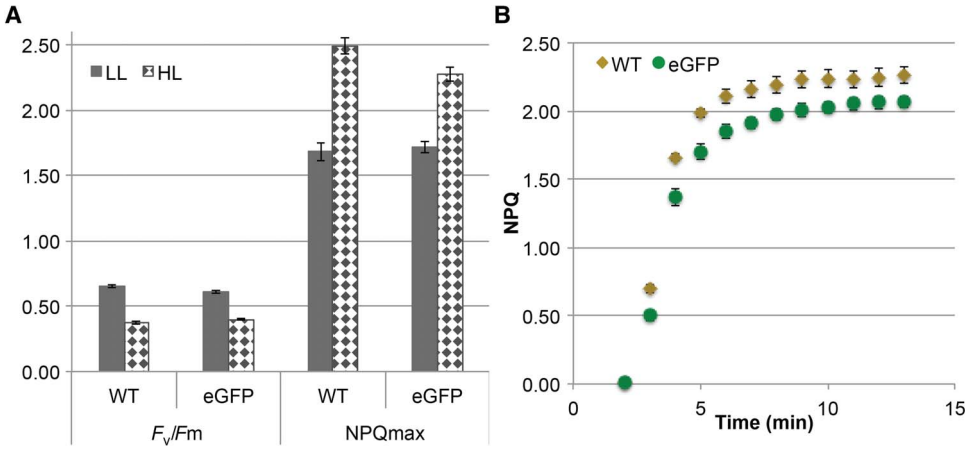

Fig. 4. Comparison of photophysiology between WT and eGFP transformant strains. (**A**) The theoretical photosynthetic efficiency and maximal NPQ level. (**B**) NPQ induction under a light intensity simulating the high-light condition in flat-panel PBRs. LL and HL represent low-light (50 μmol photons m^{-2} s^{-1}) and high-light (200 μmol photons m^{-2} s^{-1}) conditions, respectively. Values were averaged from three independent experiments. Error bars indicate SEM.

Gene ontology and gene set enrichment analysis

We performed gene set enrichment analysis (GSEA) for the up-regulated and down-regulated genes between the WT and the eGFP transformants to identify the enriched Gene Ontology (GO) terms using the Biological Networks GO tool (BiNGO) (Fig. 6A, fig. S13, and data sets S3 and S4) (*31*). The enrichment analysis revealed that up-regulated genes were significantly enriched in biological processes, including photosynthesis, generation of precursor metabolites and energy, tetrapyrrole metabolic and biosynthetic processes, porphyrin metabolic and biosynthetic processes, chlorophyll metabolic process, and protein-chromophore linkage (Fig. 6A). Cellular components (including photosystems I and II, plastid, chloroplast, and thylakoid) and molecular functions (including tetrapyrrole binding, chlorophyll binding, and heme binding) were also enriched with up-regulated genes (Fig. 6A). On the other hand, down-regulated genes were significantly involved in molecular functions, including binding of different nucleotides and nucleosides (fig. S13).

The enrichment of up-regulated DEGs (Fig. 6A) suggested that the photosynthesis process was enhanced in the eGFP transformants in comparison with the WT under the same mixed blue and red light conditions. The LHCX genes, including *LHCX1* (gene ID: Phatr3_J27278), *LHCX3* (gene ID: Phatr3_J44733), and *LHCX4* (gene ID: Phatr3_J38720), were up-regulated, whereas the *LHCX2* gene (gene ID: Phatr3_EG02404) was down-regulated at mRNA level in the eGFP transformants (data set S6). Although LHCX1 was easily detectable at protein level by Western blotting, we did not detect a significant increase in LHCX1 and LHCX3/4 at protein levels in the eGFP transformants (fig. S14 and table S2). The detected increase in the effective quantum yield, as shown in Fig. 3D, could be due to regulation of LHCX proteins at the posttranslational level (*22*, *32*, *33*) or carried out by other relevant gene products. We note that a total of 55 genes representing most of the genes involved in photosynthesis-related GO terms were up-regulated in the eGFP transformants under high-intensity light conditions (fig. S15 and data set S7).

GSEA was also performed for up-regulated and down-regulated genes in the WT to identify the enriched GO terms using BiNGO (figs. S16 and S17). The down-regulated DEGs belonging to the photosynthesis-related GO terms were significantly enriched (fig. S17), suggesting that most of the genes involved in the photosynthesis process were suppressed under high-intensity light condition compared to those under low-intensity light condition. Because light stress is one of the abiotic stressors of diatoms in the environment, DEGs that were involved in related GO terms, such as response to stress, response to oxidative stress, and response to heat, were also identified (Fig. 6B and data set S8). By analyzing the DEGs obtained from comparing the WT samples grown in high- and low-intensity light conditions, we found that six down-regulated WT genes were up-regulated, and one up-regulated WT gene was down-regulated, in the eGFP transformants under the same high-intensity light conditions (Fig. 6B and data set S8). However, GSEA indicated that only those genes involved in the GO term response to oxidative stress were significantly enriched in the WT samples, suggesting that increasing light intensity from 50 to 200 μmol photons m^{-2} s^{-1} triggered a photo-oxidative stress response in the WT (fig. S17). Together, these results indicate that the light stress–induced suppression of genes involved in photosynthesis in the WT may be mitigated in the eGFP transformants for achieving higher energy conversion efficiency and biomass productivity.

DISCUSSION

Improving photosynthesis is of considerable interest for biotechnological applications, aquaculture, and agriculture (*34*). However, for the production of biofuels, biomass, and bioactive compounds from microalgae, one of the major limitations is low photosynthetic efficiency at full sunlight or high light intensities for dense cultures (*21*). Researchers in the field have proposed some solutions to address the issue of low photosynthetic efficiency by applying flashing lights, redesigning vertical PBRs, and introducing rapid mixing in the cultivation systems for potential production at industrial scales (*35*). Here, we implemented a novel strategy, that is, the ISR, which was able to significantly increase photosynthesis efficiencies in a diatom species. We also demonstrated how ISR could boost light energy utilization in photosynthesis in diatoms and revealed the potential mechanism underlying the enhancement process so that the low-efficiency problem in photosynthetic processes may be addressed at a systems level.

Photosynthetic efficiencies in microalgae cultures are much lower than their theoretical maxima due to imbalances between the fast rate of light capture and the much slower rate of subsequent photosynthetic

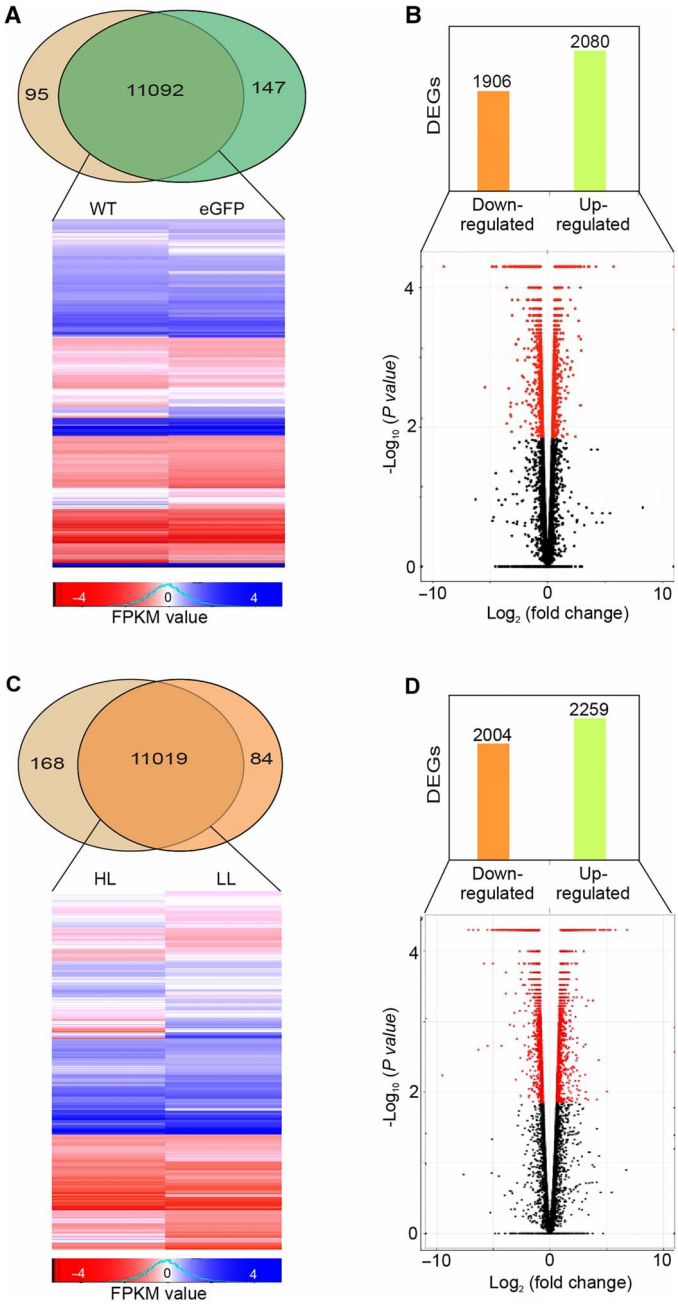

Fig. 5. Global analysis and identification of DEGs. (**A**) Genome-scale analysis of all identified genes in the eGFP transformants and WT under high-light condition. The Venn diagram indicates the numbers of shared and unique genes in the WT and eGFP transformants. The heat map compares the different profiles of gene expression levels between the WT and the eGFP transformants. (**B**) Numbers of up-regulated and down-regulated genes are shown in the eGFP transformants in comparison with the WT. (**C**) Genome-scale analysis of all identified genes between high- and low-light conditions in the WT strain. The Venn diagram indicates the numbers of shared and unique genes in high- and low-light conditions. The heat map shows the different profiles of gene expression levels between high- and low-light conditions. (**D**) The numbers of up-regulated and down-regulated genes are shown under high-light conditions in comparison with low-light conditions using the WT. For (A) and (C), values in the color bar indicate $\log_{10}$ (FPKM) values. For (B) and (D), DEGs are shown with red dots, and non-DEGs are shown with black dots in the volcano plot; the horizontal line indicates the fold changes, and the vertical line indicates the significance threshold (FDR < 0.05).

electron transfer and carbon fixation (*36*). A significant amount of the excess light energy is dissipated as heat or chlorophyll fluorescence that cannot be used by algal cells for photosynthesis (*36*). In a dense culture of algal suspensions, the algal cells at the surface, or the side exposed to the light sources, receive more light energy than they can use for the downstream carbon dioxide reduction; the excess energy is lost through heat dissipation and chlorophyll fluorescence (*21*). The algae below the surface or on the side opposite to the light sources in a PBR cannot obtain sufficient light energy due to mutual shading in algal cells (*21*). Approaches have been proposed to partially address these concurrent photoinhibition and photolimitation issues in dense cultures, such as genetic engineering techniques, to reduce the size of the light-harvesting antennae to improve light penetration and algal growth in laboratory-scale PBRs (*18*). With the development of ISR of light approach, we demonstrated that biomass production of microalgae could be improved substantially not only in flat-panel PBRs under the blue-red light regime but also, as evidenced by our pond simulator experiments, in open pond cultivations under high-intensity white light.

In addition to the enhancement of photosynthesis with flashing lights using advanced LEDs (*17*, *37*, *38*), design of PBRs through a spectral shifting of incoming lights has also improved algae growth and productivity (*27*). A previous study selected and used fluorescent dyes to modify the spectrum of the available light source for growth enhancement via a double tubular bioreactor system with a dye outside and algae inside (*27*). A more recent study showed a novel design concept by using a photoluminescent material as a backlight converter in bioreactors, and this arrangement improved the energy-harvesting efficiency in green algae (*39*). The photoluminescent spectral conversion inspired by solar photovoltaic systems has been widely applied in PBR redesign (*15*, *40*–*42*). Theoretically, direct manipulation of algae using fluorescent components may be the most efficient way for light capture and harvesting in PBRs (*43*) because it can also generate an internal light source in addition to spectral optimization and the growth performance may be enhanced by a factor of 2 (*27*). For green microalgae, engineering of PSII reaction centers in the model species *Chlamydomonas reinhardtii* has achieved optimal photosynthetic efficiencies under different solar intensities (*12*). In contrast, the ISR strategy developed in this study optimizes the incoming light spectrum internally to enhance energy efficiency by integrating fluorescent protein components genetically. The ISR approach can use existing infrastructure, such as existing PBRs and open pond systems, so that it offers more flexibility for applications and requires no PBR modification and, hence, no increase in CAPEX for its implementation for scaling-up in comparison with PBR reflector strategy.

Among the four *LHCX* genes, *LHCX1* gene was abundant and found maximally expressed under nonstressful light conditions (*44*), which suggested the *LHCX1* protein as a likely NPQ effector that modulates the excess energy dissipation and enables efficient photoprotection in diatoms in response to different environments (*44*), whereas the *LHCSR3* protein (LHC stress-related protein 3) has been well studied and demonstrated as an essential NPQ effector protein of the high-light response in *C. reinhardtii* (*45*). It has also been reported that high-light exposure induced overexpression of some LHC proteins, which promote NPQ for photoprotection in diatoms (*22*). For example, *LHCX2*, the nucleus-encoded gene for one of the antenna proteins, responds to light stress and is up-regulated under high-light conditions, promoting higher qE for photoprotection (*22*). The *LHCX* genes have been studied extensively for their potential roles in photoprotection in short-term response to high-light exposure or light quality shift (*22*, *44*). However,

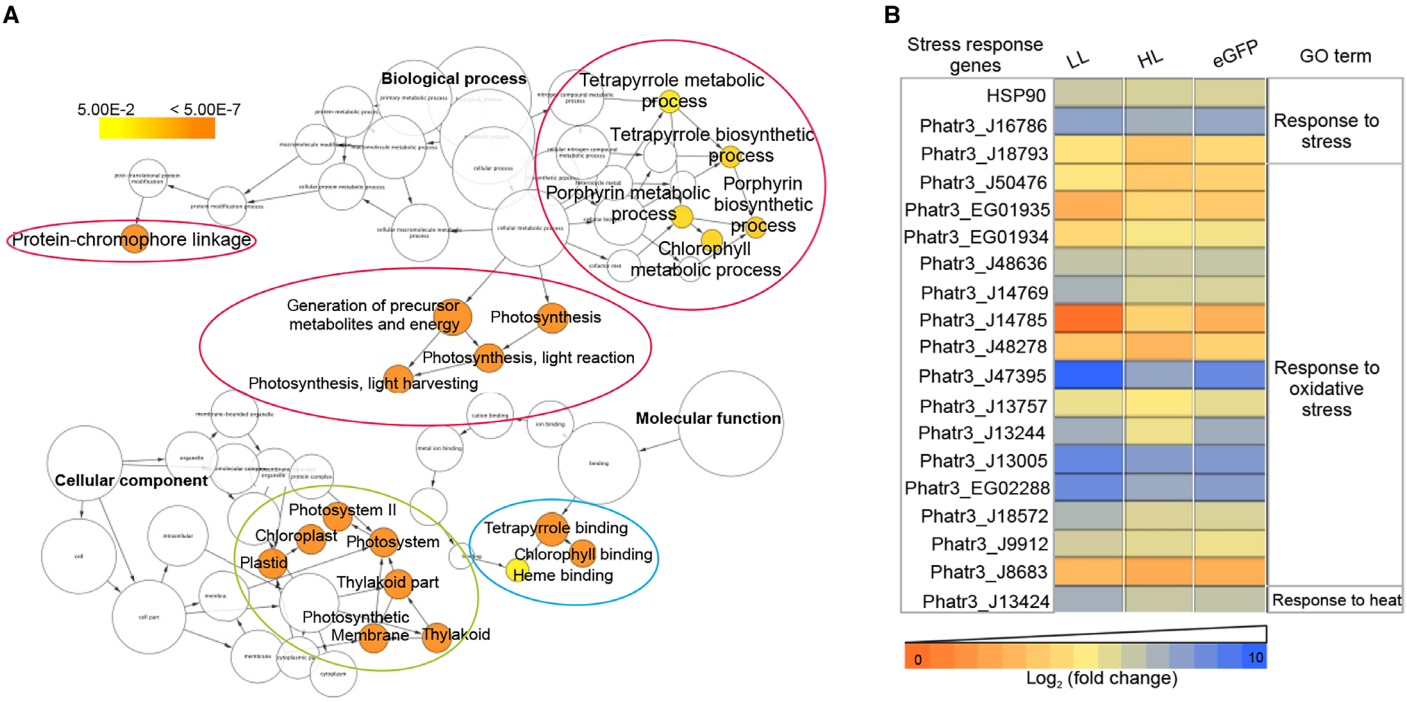

Fig. 6. Gene set enrichment analysis. (**A**) Identification of up-regulated genes highlighting the photosynthesis process in the eGFP transformants in comparison with the WT under high-intensity light condition. GO terms are represented as nodes in the graph, the color gradient (yellow to orange) represents the statistical term enrichment significance ($P < 0.05$), white (no color) indicates no significant difference, and node sizes indicate the relative numbers of genes that represent the GO term. (**B**) Identified DEGs involved in stress response in the WT strain between high- and low-intensity light conditions. The $\log_2$ (FPKM) values are shown for the WT under both high- and low-light conditions and the eGFP transformants under high-light condition.

our study showed a modest increase only at the mRNA level for *LHCX1*, *LHCX3*, and *LHCX4* genes and their uncovered quasi–steady-state expression profile under light stress conditions. Transcriptomic analysis together with LHCX protein level analysis showed different changes in transcript and protein levels and suggest that LHCX proteins may be posttranslationally modified (*22*, *32*, *33*), which is also consistent with the rapid induction that we observe in NPQ level and shift in the quantum yield (Figs. 3 and 4). Together, these results reflect the complex regulation of photoprotection in diatoms due to multiple-layer players (*33*).

In principle, the ISR strategy may be used chemically through the incorporation of fluorophores or biogenically through the expression of fluorescent proteins in diatoms. Direct incorporation of fluorescent dyes chemically into the diatom culture appears simple, but the dyes and their decomposed derivatives may have adverse effects on diatoms in the long run. In addition, the costs of introducing chemical fluorophores may be prohibitive in long-term, large-scale cultivation due to potential instability of fluorescent dyes in diatom cultures and scale of the usage. Furthermore, if the biomass is to be used for the production of nutraceutical or bioactive compounds for human and animal consumptions, inclusion of chemical fluorophores is not likely going to be an acceptable practice. Biogenic employment of ISR addresses these issues about fluorescent dyes by genetically engineering diatom cells with fluorescent proteins as controllable components due to GFPs having been widely used as labeling and imaging tools in algae and developed with relatively high stability (*11*). For ISR development, the chloroplast-localized eGFP expression may be the preferred design strategy as a close association between eGFP and the fucoxanthin-containing LHCs (LHCXs) can facilitate more efficient light energy transfers. However, we obtained higher expression levels from the cytoplasmically targeted eGFP constructs, and strong eGFP expression and its associated highly stable fluorescence are prerequisites for successful light conversion and transfer in the eGFP transformants. Further, it has been reported that the native fluorescent proteins, such as GFP, produced in corals may also play a significant role in light response and modulation of internal light environments for algal symbionts (*46*) through light spectral recomponsitioning, speculating that the ISR strategy developed in this study is analogous to a natural one evolved in these marine organisms.

Although the ISR approach developed in this study takes advantage of fucoxanthin that is present only in brown algae and diatoms, other algal groups, such as red algae (Rhodophyta), that use phycobiliproteins as accessory pigments also efficiently absorb and transfer green light energy to chlorophyll *a* (*47*). Furthermore, β-carotene, which is a common carotenoid species present in all major algal groups, such as green algae, red algae, and diatoms as well as in higher plants, can also absorb green light and transfer energy to chlorophyll, albeit at a lower energy transfer efficiency (*48*, *49*). In addition to GFPs, red fluorescent proteins (RFPs) that absorb green light and emit red fluorescence can be applied in different algal production systems using the ISR strategy developed here. RFPs with a high fluorescence quantum yield and appropriate emission spectrum can be used to maximize the light utilization in algae because chlorophyll *a* efficiently recaptures red light/fluorescence. We foresee the described approach to help in the development of superior diatoms and other algal strains for large-scale cultivation, in addition to shedding light on managing light stress in diatoms.

MATERIALS AND METHODS

Algal culture and growth conditions

The algal strain *P. tricornutum* (CCAP 1055/1, Culture Collection of Algae and Protozoa, Scottish Marine Institute, Scotland, UK) (*50*) was used in this study. The seed culture of diatom *P. tricornutum* was grown using f/2 medium (*51*) on either solid agar plates or in liquid culture (in flasks) under continuous cool white fluorescent lights of a total light intensity of 50 μmol photons m^{-2} s^{-1} at 22° ± 2°C.

Cultivation in flat-panel and OPS PBRs

The flat-panel PBR FMT 150/1000-RB was purchased from Photon Systems Instruments. The supplied blue and red LED arrays have narrow output spectra of 455 ± 24 and 627 ± 20 nm in this instrument, respectively. The PBR (*52*), with a working volume of 800-ml culture, was set up according to the manufacturer's instruction. For OPS experiments, the cultures were grown under a 14:10-hour light/dark cycle using a sinusoidal approximation of daily light with a peak intensity of 2000 μmol photons m^{-2} s^{-1}. The OPSs were approximately cylindrical PBRs (*30*) and were set up with a working volume of 360 ml and a light depth in the culture of 14.0 cm for each. To prepare the flat-panel PBR and OPS experiments, the seed culture from the flasks was first adapted to a light intensity of 50 μmol photons m^{-2} s^{-1} consisting of 75% red lights and 25% blue lights in flat-panel PBR experiments over 24 hours, which reduced the lag phase of algal growth in bioreactors. For all experiments, modified f/2 medium with additional 10 mM KNO_3 was used in PBR cultivation experiments. The PBRs were injected with air enriched with 1.0 to 2.0% CO_2 at a flow rate of 0.36 liters/min. Temperature and pH were maintained at 22° ± 2°C and 8.0 ± 0.2, respectively. Stirring was set at a constant rate of 200 rpm using a 28.6-mm stir bar. The initial cell concentration for all experiments was relatively high ($A_{627nm} \geq 1.0$), which allows sufficient absorption of incident lights by the algal culture (*53*). All growth experiments were performed either in triplicate or duplicate.

Chlorophyll fluorescence measurements for photosynthetic parameters

Chlorophyll fluorescence was measured using a MINI-PAM-II (Heinz Walz GmbH) with a KS-2500 suspension cuvette attachment. The maximum photosynthetic efficiency of PSII was determined as $F_v/F_m = (F_m - F_o)/F_m$, where F_m is the maximal fluorescence and F_o is the ground fluorescence in dark- or low light–adapted cells (*22*). For all experiments using the MINI-PAM-II, the samples were adapted to dark or dim light (less than 10 μmol photons m^{-2} s^{-1}) for 1 hour at 20°C before measurements. The maximal NPQ values for all samples were measured upon exposure to a light intensity of 1150 μmol photons m^{-2} s^{-1} for 10 min. NPQ was measured with MINI-PAM-II and calculated using the formula $NPQ = F_m/F_m' - 1$ (*22*). The effective quantum yield of PSII in cells was determined as F_v'/F_m' when exposed to different light intensities using the integrated double-modulation fluorometer in flat-panel PBRs (FMT 150/1000-RB), where F_m' is the maximum fluorescence emission level in the light-acclimated cells.

Determination of absorption and emission spectra

Absorption and emission spectra were determined using the hybrid multimode microplate reader Synergy H1 (BioTek Instruments) according to the manufacturer's manual.

Biomass determination and photosynthetic efficiency calculation

Samples were collected every 24 hours. For dry biomass measurements (*54*), typically 5 ml of cell suspension was collected on a mixed cellulose membrane (pore size, 0.45 μm), washed twice with deionized water, and dried for 24 hours at 60°C before weighing. A calibration curve was generated between the optical density and the dry biomass concentration, and then, the biomass concentration was determined by measuring the absorbance of algal culture in a microplate reader.

The photosynthetic efficiency Ψ_E is defined as the amount of energy stored in the biomass generated per unit of radiance absorbed by the culture. The equation for calculating the photosynthetic efficiency is expressed as follows

$$\Psi_E = P_b \times H_{biomass}/F_{vol}$$

where P_b stands for the volumetric biomass productivity (g $liter^{-1}$ day^{-1}), $H_{biomass}$ stands for the combustion enthalpy of the biomass (kJ g^{-1}), and F_{vol} stands for the energy of photon flux absorbed per unit volume per unit time (kJ $liter^{-1}$ day^{-1}). The combustion enthalpy $H_{biomass}$ may be directly measured or calculated from the biochemical composition and a reference value of 20.15 kJ g^{-1} dry biomass of the diatom *P. tricornutum*, which was assumed in this study. We note that the combustion energy may vary with the lipid content of algal biomass (*55*). To determine F_{vol}, the input energy consisting of 75% red lights and 25% blue lights were calculated on the basis of their energies of peak wavelengths (that is, 627 nm for the red light and 455 nm for the blue light), the specific light intensities, and the bioreactor culture volumes (*17*, *55*). We note that this method of F_{vol} calculation is valid only for highly dense cultures. The initial biomass concentration for all experiments was high ($A_{627nm} \geq 1.0$); therefore, light energy loss due to light scattering was negligible (*17*). Visual inspection of PBRs confirmed that LED lights were fully absorbed by the dense culture.

Generation of genetically modified *P. tricornutum* cells

The vectors pPha-T1/pre138-eGFP (*11*), pPhae-T1/eGFP (*11*), pPha-NR (GenBank: JN180663.1), and pKSII containing the eGFP gene sequence were used for generation of genetically modified *P. tricornutum* cells. Among these vectors, pPha-T1 (GenBank: AF219942.1) is a shuttle vector with an fcpA promoter of *P. tricornutum*, and *pre138* is the gene for the presequence of PtCA1 precursor encoding 46 N-terminal amino acids (Pre46AA), which can translocate the expressed eGFP to the chloroplast from the cytosol, whereas pPha-NR is a shuttle vector with a nitrate reductase (NR) promoter of *P. tricornutum*. A schematic map was provided to illustrate the process for generation of *P. tricornutum* transformant strains in this study (fig. S18).

For the construction of the vector pPha-NR/eGFP, primers 5′-AAGAATTCATGGTGAGCAAGGGCGAGGA-3′ (forward) and 5′-CCAAGCTTTTACTTGTACAGCTCGTCCATGC-3′ (reverse), underlined here with Eco RI and Hind III restriction sites, were used to amplify eGFP gene fragments using plasmid pKSII containing eGFP gene as a template. The polymerase chain reaction (PCR) products and the vector pPha-NR were then digested respectively using the restriction enzymes Eco RI and Hind III (New England Biolabs Inc.) according to the manufacturer's manual. After digestion, the DNA fragments were purified and ligated using T4 DNA ligase to connect pPha-NR with eGFP gene through their cohesive ends according to the manufacturer's manual. The construct pPha-NR/eGFP was then transformed into *Escherichia coli* (JM109) competent cells from Sigma-Aldrich. After selection with ampicillin (100 μg/ml), the construct pPha-NR/eGFP was then extracted from the cell culture using the Qiagen Plasmid Mini kit from Qiagen.

For transformation of different constructs with eGFP gene to the diatom *P. tricornutum*, the multipulse electroporation protocol (*56*) was

followed with slight modifications on the washing step to adjust the resistance of mixture in the cuvette. The electroporation was performed using NEPA21 electroporator (Nepa Gene Co. Ltd.). The transformed cells were selected on f/2 solid plates containing 1% agar and Zeocin (100 μg/ml) as a selection marker.

Elemental analysis of carbon fraction in dry biomass

Carbon fraction in dry biomass from PBR experiments was determined with an elemental analyzer (2400 CHNS/O Series II System, PerkinElmer) (*57*). Dry biomass samples were also analyzed using scanning electron microscope coupled with energy-dispersive spectroscopy (Quanta 450 FEG, FEI Co.) (*58*) to determine elemental carbon fraction. Both analyses were performed using biomass samples from three independent growth experiments (triplicates) under a light intensity of 200 μmol photons m^{-2} s^{-1}.

Flow cytometer experiments

Flow cytometer experiments were performed as described previously (*8*, *59*) to characterize the WT, the dye-stained WT, and the eGFP transformants based on their fluorescence signals. Staining BODIPY 505/515 and ATTO 465 were applied according to the manufacturer's manual (Sigma-Aldrich). Fluorescence intensities using different excitation wavelengths and filters were measured by flow cytometry (BD FACSAria III, BD Biosciences).

Protein extraction and Western blot analysis

Diatom samples from PBR experiments under a light intensity of 200 μmol photons m^{-2} s^{-1} were centrifuged, and cell pellets were collected and frozen at −80°C until processing. Total cellular proteins were isolated using protein extraction buffer (Agrisera Company). Western blot analyses were performed on total cell protein extracts (*33*) using primary antibodies: anti-LHCSR (a gift from K. Niyogi, University of California, Berkeley, Berkeley, CA) (1:2000) for detecting LHCX proteins and anti-AtpB (AS05 085, Agrisera Company) (1:5000) as a loading control. Western blot analyses were performed using cell samples from three independent growth experiments (triplicates).

Laser-scanning confocal microscopy

Fluorescent microscopy of chlorophyll *a* autofluorescence and eGFP fluorescence was carried out with a laser-scanning confocal microscope (*11*) using an inverted multiphoton excitation fluorescence microscope (FluoView FV 1000, Olympus). The high-frequency transduction filter 488/633 was selected as the primary dichroic splitter, and two laser lines (488 and 633 nm) were activated for the excitation of the specimen. The images were acquired using an Olympus FV 1000 confocal microscope with the following parameters: objective, 60×; numerical aperture of 1.3; laser power, 9 μW for both GFP and chlorophyll *a* autofluorescence.

RNA extraction, library preparation, and transcriptome sequencing (RNA-seq)

Three experimental groups, each in biological triplicate, were used for the RNA-seq study. The groups were the WT *P. tricornutum*, the nitrate-inducible eGFP transformants cultivated under a light intensity of 200 μmol photons m^{-2} s^{-1} (consisting of 75% red lights and 25% blue lights), and the WT grown under a low-light intensity of 50 μmol photons m^{-2} s^{-1} of the same red-blue composition. Cells for these experiments were grown in flat-panel PBRs using the aforementioned light exposure parameters. Total RNA extraction was performed using the MagMAX-96 Total RNA Isolation kit AM1830 with all necessary reagents (Thermo Fisher Scientific Inc.) according to the manufacturer's instruction. The complementary DNA (cDNA) libraries were prepared using the TruSeq RNA Library Preparation kit v2 (Illumina) according to the manufacturer's instruction. Polyadenylate-containing mRNA was purified by oligo(dT) magnetic beads from 1.0 μg of total RNA sample and fragmented using divalent cations. The cleaved RNA fragments were used for the first-strand cDNA synthesis using reverse transcriptase and random primers, followed by second-strand cDNA synthesis using DNA polymerase I and ribonuclease H. After second-strand cDNA synthesis, fragments were treated with end-repair, A-base tailing, and adapter ligation consecutively. The samples were amplified by PCR to create the final cDNA library. The concentration and size of the cDNA library were determined with a Qubit 2.0 Fluorometer (Invitrogen) and an Agilent 2100 Bioanalyzer (Agilent Technologies), respectively. After quality inspection, the library was quantified by quantitative PCR for cluster generation on the Bot system and then sequenced using paired-end sequencing of 2 × 100–base pair read length on an Illumina HiSeq 2500 system (Illumina). The RNA-seq data were deposited to the National Center for Biotechnology Information (NCBI) database with accession numbers SAMN04961176 (SRA: SRS1425240), SAMN04961177 (SRA: SRS1425243), and SAMN04961186 (SRA: SRS1425244) for each sample, respectively.

Functional annotation and analysis of gene or protein sequences

For functional annotation process and analysis of gene or protein sequences, the reference data were downloaded from Ensembl Protists database and contained 12,178 protein sequences (*Phaeodactylum_tricornutum.ASM15095v2.31.pep.all.fa*). Command line BLAST (Basic Local Alignment Search Tool) (*60*) blastp (2.2.31+) against the latest NCBI database (version 2.2.31+) was performed, with the parameter *e* value of 0.001, maximum high-scoring segment pairs of one, the total number of descriptions of one, and a total number of alignments of one. The 100% alignment was confirmed with the diatom species *P. tricornutum* in NCBI database. On the basis of the blastp results, functional annotation of *P. tricornutum* was performed using BLAST2GO (*61*), in three steps of GO mapping (*62*), functional annotation, and ANNEX.

DEGs and GSEA

The genome sequence of *P. tricornutum* (2013-07-EBI-Phatr3) was used as a reference (http://protists.ensembl.org/Phaeodactylum_tricornutum/Info/Annotation/) to align the transcriptome reads. To characterize gene expression in cells, FPKM values (*63*) were calculated, a normalized measure of read density that allows transcript levels to be compared both within and between samples quantitatively. The algorithm Cuffdiff (*64*) was used to identify DEGs between two groups of samples (triplicates within each group). Functional analysis and GSEA of DEGs were performed using BiNGO (*31*) plugin version 3.0.3 in Cytoscape. BiNGO determined the statistical overrepresentation of the DEGs genes over the GO terms. The *P* values were calculated using hypergeometric test, and Benjamini-Hochberg false discovery rate (FDR) correction was used to identify the statistical significance of GO terms with corrected $P = 0.05$ for multiple testing (*31*). The annotation file is the custom annotation based on our BLAST2GO result from the previous section (sequence alignment and functional annotation). The network was automatically laid out on the basis of BiNGO visual style, where nodes represented the GO terms, the size of the node referred to the number

of genes, and the color of the nodes reflected the enrichment significance of the words.

Statistical analysis

Student's *t* test was performed to evaluate the significance in the difference between the two groups of samples for growth data ($P < 0.05$).

SUPPLEMENTARY MATERIALS

Supplementary material for this article is available at http://advances.sciencemag.org/cgi/content/full/3/9/e1603096/DC1

fig. S1. Effects of the dye ATTO 465 on the shifting of absorption spectrum in *P. tricornutum* cell suspensions.
fig. S2. Effects of the dye BODIPY 505/515 on the shifting of absorption spectrum in *P. tricornutum* cell suspensions.
fig. S3. Evaluation of the biocompatibility of fluorescence dyes after staining for 30 min.
fig. S4. Photostability of fluorescent BODIPY 505/515 staining on diatom cells within 24 hours.
fig. S5. Fluorescent microscopy images of the WT and eGFP transformants of *P. tricornutum* cells.
fig. S6. Selection of positive eGFP transformants.
fig. S7. Comparison of growth performance between the WT and the chloroplast-localized eGFP transformants over 24 hours using flat-panel PBRs.
fig. S8. The enhancement of green fluorescence in the eGFP transformants.
fig. S9. The regain of green fluorescence in the nitrate-inducible eGFP transformants upon presence of 5 mM nitrate (KNO_3).
fig. S10. Comparison of growth performance between the WT and the nitrate-inducible eGFP transformants over 24 hours using flat-panel PBRs.
fig. S11. The light supply setup of OPSs.
fig. S12. Cultivation of diatoms in OPSs.
fig. S13. GSEA of down-regulated DEGs in the eGFP transformants.
fig. S14. Analysis of LHCX proteins by Western blotting in cells under high-intensity light condition.
fig. S15. Heat map of expression profile of DEGs based on RNA-seq data in relation to photosynthesis.
fig. S16. GSEA of up-regulated genes between low- and high-intensity light conditions through BiNGO.
fig. S17. GSEA of down-regulated genes between low- and high-intensity light conditions through BiNGO.
fig. S18. A schematic process for generation of genetically modified *P. tricornutum* strains.
table S1. Carbon fraction analysis in dry biomass.
table S2. Comparison of detected level of LHCX proteins between the WT and the eGFP transformants.
data set S1. Shared genes between the WT and the eGFP transformants under high-intensity light condition.
data set S2. Genes uniquely present in the eGFP transformants under high-intensity light condition.
data set S3. GSEA of up-regulated genes in the eGFP transformants under high-intensity light condition.
data set S4. GSEA of down-regulated genes in the eGFP transformants under high-intensity light condition.
data set S5. List of DEGs in the WT under high-light intensity condition compared to that under low-intensity light condition.
data set S6. Key identified genes involved in photosynthesis.
data set S7. List of identified genes in relation to photosynthesis, as shown in fig. S14.
data set S8. DEGs involved in stress response in the WT based on high- and low-intensity light conditions.

REFERENCES AND NOTES

1. J. T. Pronk, S. Y. Lee, J. Lievense, J. Pierce, B. Palsson, M. Uhlen, J. Nielsen, How to set up collaborations between academia and industrial biotech companies. *Nat. Biotechnol.* **33**, 237–240 (2015)
2. P. Falkowski, Ocean science: The power of plankton. *Nature* **483**, S17–S20 (2012).
3. D. Singh, R. Carlson, D. Fell, M. Poolman, Modelling metabolism of the diatom *Phaeodactylum tricornutum*. *Biochem. Soc. Trans.* **43**, 1182–1186 (2015).
4. C. M. Gatenby, D. M. Orcutt, D. A. Kreeger, B. C. Parker, V. A. Jones, R. J. Neves, Biochemical composition of three algal species proposed as food for captive freshwater mussels. *J. Appl. Phycol.* **15**, 1–11 (2003).
5. M. Hlavova, Z. Turoczy, K. Bisova, Improving microalgae for biotechnology—From genetics to synthetic biology. *Biotechnol. Adv.* **33**, 1194–1203 (2015).
6. O. Levitan, J. Dinamarca, G. Hochman, P. G. Falkowski, Diatoms: A fossil fuel of the future. *Trends Biotechnol.* **32**, 117–124 (2014).
7. A. Bozarth, U.-G. Maier, S. Zauner, Diatoms in biotechnology: Modern tools and applications. *Appl. Microbiol. Biotechnol.* **82**, 195–201 (2009).
8. F. Daboussi, S. Leduc, A. Maréchal, G. Dubois, V. Guyot, C. Perez-Michaut, A. Amato, A. Falciatore, A. Juillerat, M. Beurdeley, D. F. Voytas, L. Cavarec, P. Duchateau, Genome engineering empowers the diatom *Phaeodactylum tricornutum* for biotechnology. *Nat. Commun.* **5**, 3831 (2014).
9. R. León-Bañares, D. González-Ballester, A. Galván, E. Fernández, Transgenic microalgae as green cell-factories. *Trends Biotechnol.* **22**, 45–52 (2004).
10. O. Levitan, J. Dinamarca, E. Zelzion, M. Y. Gorbunov, P. G. Falkowski, An RNA interference knock-down of nitrate reductase enhances lipid biosynthesis in the diatom *Phaeodactylum tricornutum*. *Plant J.* **84**, 963–973 (2015).
11. Y. Tanaka, D. Nakatsuma, H. Harada, M. Ishida, Y. Matsuda, Localization of soluble β-carbonic anhydrase in the marine diatom *Phaeodactylum tricornutum*. Sorting to the chloroplast and cluster formation on the girdle lamellae. *Plant Physiol.* **138**, 207–217 (2005).
12. D. J. Vinyard, J. Gimpel, G. M. Ananyev, S. P. Mayfield, G. C. Dismukes, Engineered Photosystem II reaction centers optimize photochemistry versus photoprotection at different solar intensities. *J. Am. Chem. Soc.* **136**, 4048–4055 (2014).
13. W.-H. Xie, C.-C. Zhu, N.-S. Zhang, D.-W. Li, W.-D. Yang, J.-S. Liu, R. Sathishkumar, H.-Y. Li, Construction of novel chloroplast expression vector and development of an efficient transformation system for the diatom *Phaeodactylum tricornutum*. *Mar. Biotechnol.* **16**, 538–546 (2014).
14. J. A. Del Campo, M. García-González, M. G. Guerrero, Outdoor cultivation of microalgae for carotenoid production: Current state and perspectives. *Appl. Microbiol. Biotechnol.* **74**, 1163–1174 (2007).
15. H. D. Amrei, R. Ranjbar, S. Rastegar, B. Nasernejad, A. Nejadebrahim, Using fluorescent material for enhancing microalgae growth rate in photobioreactors. *J. Appl. Phycol.* **27**, 67–74 (2015).
16. A. F. Clarens, E. P. Resurreccion, M. A. White, L. M. Colosi, Environmental life cycle comparison of algae to other bioenergy feedstocks. *Environ. Sci. Technol.* **44**, 1813–1819 (2010).
17. W. Fu, O. Gudmundsson, A. M. Feist, G. Herjolfsson, S. Brynjolfsson, B. Ø Palsson, Maximizing biomass productivity and cell density of *Chlorella vulgaris* by using light-emitting diode-based photobioreactor. *J. Biotechnol.* **161**, 242–249 (2012).
18. Z. Perrine, S. Negi, R. T. Sayre, Optimization of photosynthetic light energy utilization by microalgae. *Algal Res.* **1**, 134–142 (2012).
19. I. G. Anemaet, M. Bekker, K. J. Hellingwerf, Algal photosynthesis as the primary driver for a sustainable development in energy, feed, and food production. *Mar. Biotechnol.* **12**, 619–629 (2010).
20. G. G. Zaimes, V. Khanna, Microalgal biomass production pathways: Evaluation of life cycle environmental impacts. *Biotechnol. Biofuels* **6**, 88 (2013).
21. K. Wichuk, S. Brynjólfsson, W. Fu, Biotechnological production of value-added carotenoids from microalgae: Emerging technology and prospects. *Bioengineered* **5**, 204–208 (2014).
22. B. Lepetit, S. Sturm, A. Rogato, A. Gruber, M. Sachse, A. Falciatore, P. G. Kroth, J. Lavaud, High light acclimation in the secondary plastids containing diatom *Phaeodactylum tricornutum* is triggered by the redox state of the plastoquinone pool. *Plant Physiol.* **161**, 853–865 (2013).
23. P. Kuczynska, M. Jemiola-Rzeminska, K. Strzalka, Photosynthetic pigments in diatoms. *Mar. Drugs* **13**, 5847–5881 (2015).
24. M. Herbstová, D. Bína, P. Koník, Z. Gardian, F. Vácha, R. Litvín, Molecular basis of chromatic adaptation in pennate diatom *Phaeodactylum tricornutum*. *Biochim. Biophys. Acta* **1847**, 534–543 (2015).
25. G. E. Hoffman, M. V. Sanchez-Puerta, C. F. Delwiche, Evolution of light-harvesting complex proteins from Chl *c*-containing algae. *BMC Evol. Biol.* **11**, 101 (2011).
26. H. Wagner, T. Jakob, C. Wilhelm, Balancing the energy flow from captured light to biomass under fluctuating light conditions. *New Phytol.* **169**, 95–108 (2006).
27. A. Prokop, M. F. Quinn, M. Fekri, M. Murad, S. A. Ahmed, Spectral shifting by dyes to enhance algae growth. *Biotechnol. Bioeng.* **26**, 1313–1322 (1984).
28. J. Rumin, H. Bonnefond, B. Saint-Jean, C. Rouxel, A. Sciandra, O. Bernard, J.-P. Cadoret, G. Bougaran, The use of fluorescent Nile red and BODIPY for lipid measurement in microalgae. *Biotechnol. Biofuels* **8**, 42 (2015).
29. F. Hempel, U. G. Maier, An engineered diatom acting like a plasma cell secreting human IgG antibodies with high efficiency. *Microb. Cell Fact.* **11**, 126 (2012).
30. B. F. Lucker, C. C. Hall, R. Zegarac, D. M. Kramer, The environmental photobioreactor (ePBR): An algal culturing platform for simulating dynamic natural environments. *Algal Res.* **6**, 242–249 (2014).
31. S. Maere, K. Heymans, M. Kuiper, BiNGO: A Cytoscape plugin to assess overrepresentation of Gene Ontology categories in biological networks. *Bioinformatics* **21**, 3448–3449 (2005).

32. M. Grabsztunowicz, M. M. Koskela, P. Mulo, Post-translational modifications in regulation of chloroplast function: Recent advances. *Front. Plant Sci.* **8**, 240 (2017).
33. L. Taddei, G. R. Stella, A. Rogato, B. Bailleul, A. E. Fortunato, R. Annunziata, R. Sanges, M. Thaler, B. Lepetit, J. Lavaud, M. Jaubert, G. Finazzi, J.-P. Bouly, A. Falciatore, Multisignal control of expression of the LHCX protein family in the marine diatom *Phaeodactylum tricornutum*. *J. Exp. Bot.* **67**, 3939–3951 (2016).
34. X.-G. Zhu, S. P. Long, D. R. Ort, Improving photosynthetic efficiency for greater yield. *Annu. Rev. Plant Biol.* **61**, 235–261 (2010).
35. M. Heining, R. Buchholz, Photobioreactors with internal illumination – A survey and comparison. *Biotechnol. J.* **10**, 1131–1137 (2015).
36. L. Wobbe, C. Remacle, Improving the sunlight-to-biomass conversion efficiency in microalgal biofactories. *J. Biotechnol.* **201**, 28–42 (2015).
37. S. Abu-Ghosh, D. Fixler, Z. Dubinsky, D. Iluz, Continuous background light significantly increases flashing-light enhancement of photosynthesis and growth of microalgae. *Bioresour. Technol.* **187**, 144–148 (2015).
38. S. Abu-Ghosh, D. Fixler, Z. Dubinsky, A. Solovchenko, M. Zigman, Y. Yehoshua, D. Iluz, Flashing light enhancement of photosynthesis and growth occurs when photochemistry and photoprotection are balanced in *Dunaliella salina*. *Eur. J. Phycol.* **50**, 469–480 (2015).
39. L. Wondraczek, M. Batentschuk, M. A. Schmidt, R. Borchardt, S. Scheiner, B. Seemann, P. Schweizer, C. J. Brabec, Solar spectral conversion for improving the photosynthetic activity in algae reactors. *Nat. Commun.* **4**, 2047 (2013).
40. E. Sforza, E. Barbera, A. Bertucco, Improving the photoconversion efficiency: An integrated photovoltaic-photobioreactor system for microalgal cultivation. *Algal Res.* **10**, 202–209 (2015).
41. A. M. Detweiler, C. E. Mioni, K. L. Hellier, J. J. Allen, S. A. Carter, B. M. Bebout, E. E. Fleming, C. Corrado, L. E. Prufert-Bebout, Evaluation of wavelength selective photovoltaic panels on microalgae growth and photosynthetic efficiency. *Algal Res.* **9**, 170–177 (2015).
42. L. Wondraczek, E. Tyystjärvi, J. Méndez-Ramos, F. A. Müller, Q. Zhang, Shifting the sun: Solar spectral conversion and extrinsic sensitization in natural and artificial photosynthesis. *Adv. Sci.* **2**, 1500218 (2015).
43. J. Gressel, D. Eisenstadt, D. Schatz, S. Einbinder, S. Ufaz, Use of fluorescent protein in cyanobacteria and algae for improving photosynthesis and preventing cell damage, U.S. Patent 12/586,185 (2010).
44. B. Bailleul, A. Rogato, A. de Martino, S. Coesel, P. Cardol, C. Bowler, A. Falciatore, G. Finazzi, An atypical member of the light-harvesting complex stress-related protein family modulates diatom responses to light. *Proc. Natl. Acad. Sci. U.S.A.* **107**, 18214–18219 (2010).
45. D. Petroutsos, R. Tokutsu, S. Maruyama, S. Flori, A. Greiner, L. Magneschi, L. Cusant, T. Kottke, M. Mittag, P. Hegemann, G. Finazzi, J. Minagawa, A blue-light photoreceptor mediates the feedback regulation of photosynthesis. *Nature* **537**, 563–566 (2016).
46. M. S. Roth, M. I. Latz, R. Goericke, D. D. Deheyn, Green fluorescent protein regulation in the coral *Acropora yongei* during photoacclimation. *J. Exp. Biol.* **213**, 3644–3655 (2010).
47. J.-C. Thomas, C. Passaquet, Characterization of a phycoerythrin without α-subunits from a unicellular red alga. *J. Biol. Chem.* **274**, 2472–2482 (1999).
48. D. M. M. Kleinegris, M. A. van Es, M. Janssen, W. A. Brandenburg, R. H. Wijffels, Carotenoid fluorescence in *Dunaliella salina*. *J. Appl. Phycol.* **22**, 645–649 (2010).
49. A. Telfer, What is β–carotene doing in the photosystem II reaction centre? *Philos. Trans. R. Soc. Lond. B Biol. Sci.* **357**, 1431–1439 (2002).
50. C. Bowler, A. E. Allen, J. H. Badger, J. Grimwood, K. Jabbari, A. Kuo, U. Maheswari, C. Martens, F. Maumus, R. P. Otillar, E. Rayko, A. Salamov, K. Vandepoele, B. Beszteri, A. Gruber, M. Heijde, M. Katinka, T. Mock, K. Valentin, F. Verret, J. A. Berges, C. Brownlee, J.-P. Cadoret, A. Chiovitti, C. J. Choi, S. Coesel, A. De Martino, J. C. Detter, C. Durkin, A. Falciatore, J. Fournet, M. Haruta, M. J. J. Huysman, B. D. Jenkins, K. Jiroutova, R. E. Jorgensen, Y. Joubert, A. Kaplan, N. Kröger, P. G. Kroth, J. La Roche, E. Lindquist, M. Lommer, V. Martin-Jézéquel, P. J. Lopez, S. Lucas, M. Mangogna, K. McGinnis, L. K. Medlin, A. Montsant, M.-P. Oudot-Le Secq, C. Napoli, M. Obornik, M. S. Parker, J.-L. Petit, B. M. Porcel, N. Poulsen, M. Robison, L. Rychlewski, T. A. Rynearson, J. Schmutz, H. Shapiro, M. Siaut, M. Stanley, M. R. Sussman, A. R. Taylor, A. Vardi, P. von Dassow, W. Vyverman, A. Willis, L. S. Wyrwicz, D. S. Rokhsar, J. Weissenbach, E. V. Armbrust, B. R. Green, Y. Van de Peer, I. V. Grigoriev, The *Phaeodactylum* genome reveals the evolutionary history of diatom genomes. *Nature* **456**, 239–244 (2008).
51. P. D. Weyman, K. Beeri, S. C. Lefebvre, J. Rivera, J. K. McCarthy, A. L. Heuberger, G. Peers, A. E. Allen, C. L. Dupont, Inactivation of *Phaeodactylum tricornutum* urease gene using transcription activator-like effector nuclease-based targeted mutagenesis. *Plant Biotechnol. J.* **13**, 460–470 (2015).
52. L. Nedbal, M. Trtílek, J. Cervený, O. Komárek, H. B. Pakrasi, A photobioreactor system for precision cultivation of photoautotrophic microorganisms and for high-content analysis of suspension dynamics. *Biotechnol. Bioeng.* **100**, 902–910 (2008).
53. W. Fu, Ó. Guðmundsson, G. Paglia, G. Herjólfsson, Ó. S. Andrésson, B. Ø. Palsson, S. Brynjólfsson, Enhancement of carotenoid biosynthesis in the green microalga *Dunaliella salina* with light-emitting diodes and adaptive laboratory evolution. *Appl. Microbiol. Biotechnol.* **97**, 2395–2403 (2013).
54. Z. Yi, M. Xu, M. Magnusdottir, Y. Zhang, S. Brynjolfsson, W. Fu, Photo-oxidative stress-driven mutagenesis and adaptive evolution on the marine diatom *Phaeodactylum tricornutum* for enhanced carotenoid accumulation. *Mar. Drugs* **13**, 6138–6151 (2015).
55. F. G. Acién Fernández, D. O. Hall, E. Cañizares Guerrero, K. Krishna Rao, E. Molina Grima, Outdoor production of *Phaeodactylum tricornutum* biomass in a helical reactor. *J. Biotechnol.* **103**, 137–152 (2003).
56. M. Miyahara, M. Aoi, N. Inoue-Kashino, Y. Kashino, K. Ifuku, Highly efficient transformation of the diatom *Phaeodactylum tricornutum* by multi-pulse electroporation. *Biosci. Biotechnol. Biochem.* **77**, 874–876 (2013).
57. T.-Y. Ho, A. Quigg, Z. V. Finkel, A. J. Milligan, K. Wyman, P. G. Falkowski, F. M. M. Morel, The elemental composition of some marine phytoplankton. *J. Phycol.* **39**, 1145–1159 (2003).
58. T. Leonardo, E. Farhi, A.-M. Boisson, J. Vial, P. Cloetens, S. Bohic, C. Rivasseau, Determination of elemental distribution in green micro-algae using synchrotron radiation nano X-ray fluorescence (SR-nXRF) and electron microscopy techniques – Subcellular localization and quantitative imaging of silver and cobalt uptake by *Coccomyxa actinabiotis*. *Metallomics* **6**, 316–329 (2014).
59. M. Terashima, E. S. Freeman, R. E. Jinkerson, M. C. Jonikas, A fluorescence-activated cell sorting-based strategy for rapid isolation of high-lipid *Chlamydomonas* mutants. *Plant J.* **81**, 147–159 (2015).
60. S. F. Altschul, W. Gish, W. Miller, E. W. Myers, D. J. Lipman, Basic local alignment search tool. *J. Mol. Biol.* **215**, 403–410 (1990).
61. A. Conesa, S. Götz, J. M. García-Gómez, J. Terol, M. Talón, M. Robles, Blast2GO: A universal tool for annotation, visualization and analysis in functional genomics research. *Bioinformatics* **21**, 3674–3676 (2005).
62. M. Ashburner, C. A. Ball, J. A. Blake, D. Botstein, H. Butler, J. M. Cherry, A. P. Davis, K. Dolinski, S. S. Dwight, J. T. Eppig, M. A. Harris, D. P. Hill, L. Issel-Tarver, A. Kasarskis, S. Lewis, J. C. Matese, J. E. Richardson, M. Ringwald, G. M. Rubin, G. Sherlock, Gene Ontology: Tool for the unification of biology. *Nat. Genet.* **25**, 25–29 (2000).
63. C. Robert, M. Watson, Errors in RNA-Seq quantification affect genes of relevance to human disease. *Genome Biol.* **16**, 177 (2015).
64. C. Trapnell, D. G. Hendrickson, M. Sauvageau, L. Goff, J. L. Rinn, L. Pachter, Differential analysis of gene regulation at transcript resolution with RNA-seq. *Nat. Biotechnol.* **31**, 46–53 (2013).

Acknowledgments: We thank M. Arnoux and Center for Genomics and Systems Biology (CGSB) Sequencing Core for the high-throughput sequencing, N. Drou and CGSB Bioinformatics Core for the RNA-seq data processing, and New York University Abu Dhabi (NYUAD) High Performance Computing and Core Technology Platforms. We thank L. Li, J. Weston, and D. Al-Khairy for their help and support in the biomass sample analysis. We also thank Y. Matsuda (Kwansei-Gakuin University) for providing the pPha-T1/pre138-EGFP and pPhae-T1/EGFP vectors, U. G. Maier (Philipps-Universität Marburg) for providing the pPha-NR and pKSII vectors, and K. Niyogi (University of California, Berkeley, Berkeley, CA) for providing the anti-LHCSR antibody. **Funding:** Financial support for this work was provided by NYUAD Faculty Research Funds (AD060), an NYUAD Institute grant (G1205-1205i), and an Al-Jalila Foundation award (21S096) to A.A. **Author contributions**: W.F. and K.S.-A. designed the research and wrote the manuscript. W.F. performed the laboratory experiments, including the vector construction, transformation, and strain validation, and bioreactor growth experiments and analyzed the data. W.F., A.C., B.K., and A.J. performed the transcriptome analysis. M.S. performed the confocal microscopy experiments. W.F., A.A.-H., B.B., and A.A. conducted the Western blotting analyses. W.F. and M.S. performed the RNA-seq experiments. W.F. and K.S.-A. drafted the manuscript with contributions from the rest of the authors. **Competing interests:** The authors declare that they have no competing interests. **Data and materials availability:** All data needed to evaluate the conclusions are present in the paper and/or the Supplementary Materials. All the original RNA-seq data were deposited to the NCBI database with accession numbers SAMN04961176 (SRA: SRS1425240), SAMN04961177 (SRA: SRS1425243), and SAMN04961186 (SRA: SRS1425244) for each group of samples, respectively. Additional data related to this paper may be requested from the authors.

Submitted 7 December 2016
Accepted 5 August 2017
Published 1 September 2017
10.1126/sciadv.1603096

Citation: W. Fu, A. Chaiboonchoe, B. Khraiwesh, M. Sultana, A. Jaiswal, K. Jijakli, D. R. Nelson, A. Al-Hrout, B. Baig, A. Amin, K. Salehi-Ashtiani, Intracellular spectral recompositioning of light enhances algal photosynthetic efficiency. *Sci. Adv.* **3**, e1603096 (2017).